

# Wide-band acoustic collimating by phononic crystal composites

Jinjie Shi, Sz-Chin Steven Lin, and Tony Jun Huang<sup>a)</sup>

Department of Engineering Science and Mechanics, The Pennsylvania State University, University Park, Pennsylvania 16802, USA

(Received 11 October 2007; accepted 8 January 2008; published online 17 March 2008)

We numerically investigated the collimation phenomena in phononic crystal (PC) composites, a sequenced series of PCs with the same period but different filling ratios. The plane wave expansion (PWE) method was used to obtain the band diagrams and the equal frequency surfaces of both single PCs and PC composites. The finite difference time domain (FDTD) method was then utilized to simulate the propagation of acoustic waves inside a PC composite. The results from both PWE calculations and FDTD simulations show that in comparison to a single PC, a PC composite can significantly enlarge the collimation region and realize wide-band acoustic collimation. © 2008 American Institute of Physics. [DOI: 10.1063/1.2895019]

Photonic crystals are periodic structures that manipulate the propagation of electromagnetic waves, much like the periodic potential in a semiconductor crystal affects the motion of electrons.<sup>1,2</sup> In the last decade, photonic crystals have attracted much interest, and many interesting phenomena (such as band gaps, negative refraction, focusing, and photon tunneling) have been observed in these structures.<sup>3-7</sup> Recently, it has been shown that photonic crystals can be used to achieve the collimation of electromagnetic waves at particular frequencies.<sup>8-10</sup> Since traditional collimation lenses made of convex and concave lenses are bulky, expensive, and hard to fabricate, photonic crystal-based collimation lenses could prove advantageous in many applications, especially in micro-nanosystems where fabricating small-scale, convex or concave lenses is challenging.

The concept of collimation can be extended to phononic crystals (PCs), which are the acoustic analogs of photonic crystals. Numerical simulation has shown that acoustic waves within a narrow band tend to be collimated or guided into the direction in which propagation is allowed.<sup>11</sup> Recently, Qiu and Liu have numerically investigated how the resonant cavities formed by line defects in PCs affect sound collimation and signal enhancement.<sup>12</sup> These methods have paved an avenue for PC-based acoustic collimation; however, they only work within a narrow frequency band, and thus are not practical for many applications. In this letter, we present a design that is capable of achieving acoustic collimation in a wide frequency range via PC composites, a sequenced series of PCs that have the same period but different filling ratios.

The two-dimensional PCs employed were composed of rigid steel cylinders arranged in a square lattice and immersed in water. The material parameters were  $\rho = 7.67 \text{ g/cm}^3$ ,  $C_L = 6.01 \text{ km/s}$ , and  $C_T = 3.23 \text{ km/s}$  for steel, and  $\rho = 1.0 \text{ g/cm}^3$  and  $C_L = 1.49 \text{ km/s}$  for water.  $\rho$  is the density and  $C_L$  and  $C_T$  represent longitudinal and transverse speeds of sound, respectively. All calculations and simulations in this letter were based on the plane wave expansion<sup>13-16</sup> (PWE) and finite difference time domain (FDTD) methods.<sup>17,18</sup> Figure 1(a) shows the calculated band diagram of two PCs, PC<sub>1</sub> (filling ratio FR=0.545) and PC<sub>2</sub>

(FR=0.442), using  $121 \times 121$  plane waves. The normalized frequency for the first full band gap of PC<sub>1</sub> ranged from 0.504 to 0.650, corresponding to points  $M_1$  and  $X_2$ , respectively. As shown in Fig. 1(a), the band gap of PC<sub>1</sub> in the  $\Gamma X$  orientation extends from point  $X_1$  (normalized frequency = 0.333) to  $X_2$ . Waves in the frequency range between  $X_1$  and  $M_1$  are inhibited in the  $\Gamma X$  orientation.

The ability achieve collimation is realized at flatbands of PC structures because acoustic waves propagate perpendicularly to the equal frequency surface (EFS) of the structure, this phenomenon is described by the following equation:

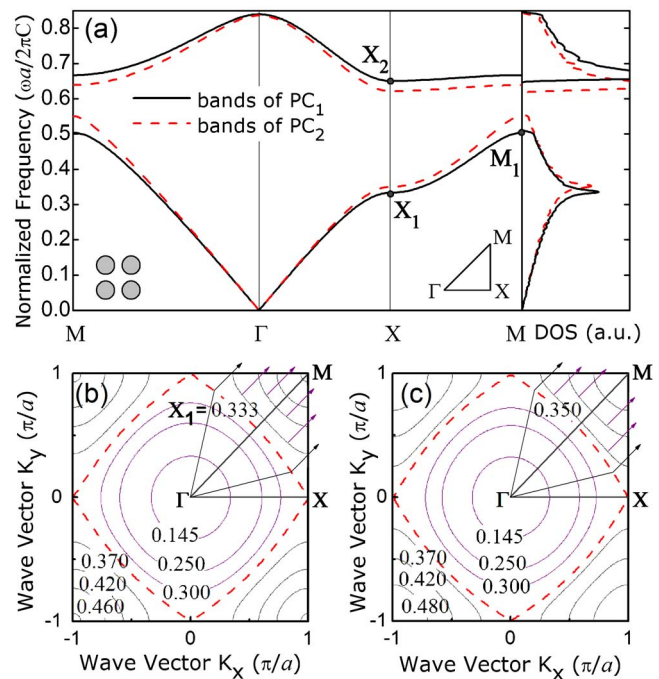


FIG. 1. (Color online) (a) Band structure (left) and density of states (DOS, right) of square-lattice PCs composed of steel cylinders in water with filling ratios of 0.545 (PC<sub>1</sub>) and 0.442 (PC<sub>2</sub>). The frequency was normalized by  $2\pi C/a$ , where  $a$  is the lattice constant and  $C$  is the sound velocity in water. (b) and (c) are the EFS of PC<sub>1</sub> and PC<sub>2</sub>, respectively. The red dotted lines represent the maximum collimation points and the arrows indicate the boundaries for the collimation region at different frequencies.

<sup>a)</sup> Author to whom correspondence should be addressed. Electronic mail: junhuang@psu.edu.

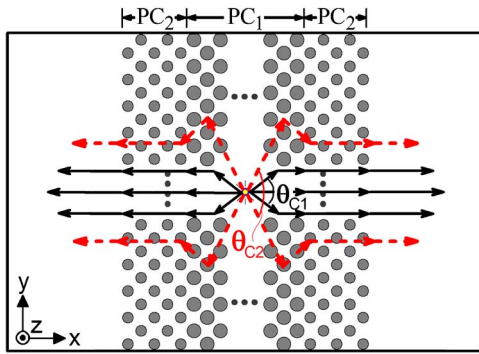


FIG. 2. (Color online) Schematic of an acoustic collimation lens comprising two PCs of the same period but different filling ratios.

$$v_g = \nabla_k[\omega(k)],$$

where  $v_g$  is the group velocity,  $\omega(k)$  is the angular frequency, and  $k$  is the wave vector. Here we show PC structures demonstrate flatbands in a certain frequency region where incident waves collimate normal to the flatband [Figs. 1(b) and 1(c)]. As shown in Fig. 1(b), at point  $X_1$  in the first band of  $PC_1$ , the curvature of the EFS is nearly zero. This implies that  $X_1$  is at the region of maximum collimation (indicated by black arrows at the boundaries of the collimation region), where the incident waves will be directed along the  $\Gamma M$  orientation. Moreover, the density of states (DOS), number of the compositions of  $(k_x, k_y)$  at a certain angular frequency [Fig. 1(a)], is inversely proportional to the curvature of the dispersion curve. Therefore, point  $X_1$  gives the maximum DOS, and incident waves with a range of wave numbers can be collimated at point  $X_1$ .

Although acoustic collimation can be achieved through a single PC structure, such a collimation system can only work over a narrow frequency range. As the frequency deviates from point  $X_1$ , the contour of the EFS will change into a circular geometry, and only a small portion of the EFS depicts a near-zero curvature [Figs. 1(b) and 1(c)]. Such circular geometries permit only waves within a certain incident angle  $\theta_c$  to be collimated, thereby limiting the use of single PC-based acoustic collimation lenses. We devised a wide-band acoustic collimation lens that is composed of a series of PCs having the same period but different filling ratios (Fig. 2). When acoustic waves pass through the first PC ( $PC_1$ , FR=0.545), the incident waves within the critical angle  $\theta_{c1}$  are collimated along the  $\Gamma M$  orientation, and remain unchanged as they propagate through the second PC ( $PC_2$ , FR=0.442). Although not collimated by  $PC_1$ , the waves outside the critical angle  $\theta_{c1}$  refract toward the center (negative refraction)<sup>19–22</sup> as they pass through  $PC_1$ . Following that, the refracted waves of original incident angle less than the critical angle  $\theta_{c2}$  ( $\theta_{c2} > \theta_{c1}$ ) will be collimated upon propagation through  $PC_2$ . Therefore, the PC composite ( $PC_1+PC_2$ ) provides an effective means to enlarge the critical incident angle. It serves as the basis of an acoustic collimation lens that focuses waves of a wide frequency range.

To reduce the boundary effects between  $PC_1$  and  $PC_2$ , the cylinders in both  $PC_1$  and  $PC_2$  were oriented in a similar fashion, and the last column of  $PC_1$  was positioned exactly at the periodic frame of  $PC_2$  (Fig. 2). In order to illustrate how a PC composite affects the collimation characteristics, we calculated the total critical angle (the maximum incident angle within which all refracted waves are less than  $5^\circ$  with

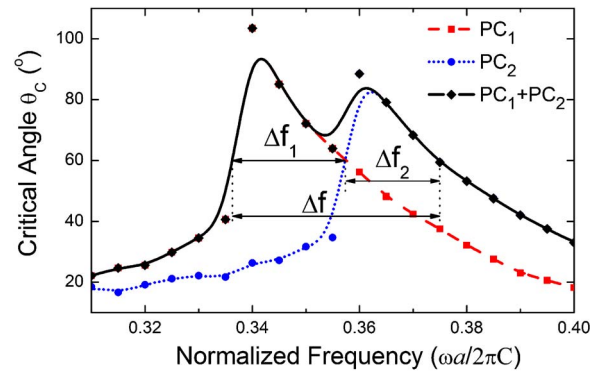


FIG. 3. (Color online) The dependence of critical angles at normalized frequency for  $PC_1$ ,  $PC_2$ , and  $PC_1+PC_2$ .  $\Delta f_1$ ,  $\Delta f_2$ , and  $\Delta f$  are the calculated collimation regions for  $PC_1$ ,  $PC_2$ , and  $PC_1+PC_2$ , respectively, assuming  $\theta_c=60^\circ$ .

respect to the  $\Gamma M$  orientation) at different frequencies for  $PC_1$ ,  $PC_2$ , and  $PC_1+PC_2$  [Fig. 3]. At  $\theta_c=60^\circ$ , the normalized frequency ranges of the collimation regions for  $PC_1$ ,  $PC_2$ , and  $PC_1+PC_2$  were calculated to be 0.336–0.357 ( $\Delta f_1$ ), 0.357–0.375 ( $\Delta f_2$ ), and 0.336–0.375 ( $\Delta f$ ), respectively. Hence, the PC composite significantly enlarges the range of the collimation region ( $\Delta f/\Delta f_1=185\%$  and  $\Delta f/\Delta f_2=220\%$ ). We anticipate that when using a series ( $>2$ ) of PCs, the range of the collimation region can be further improved.

To verify the calculated results based on the PWE method, we employed the FDTD method to simulate the collimation phenomena of a PC composite within the collimation region ( $\Delta f=0.336-0.375$ ). Figure 4(a) is a schematic of the PC composite used in the FDTD simulation with a point source placed in the center of the composite. The lattice constant  $a$  was assumed to be 8 mm, the size of the PC composite was  $30a \times 20a$ , and other parameters used in the FDTD simulations were the same as those in the PWE calculations. The simulation results [Figs. 4(b)–4(d)] showed clear collimation phenomena at three different normalized frequencies (0.340, 0.355, and 0.370) within the collimation region.

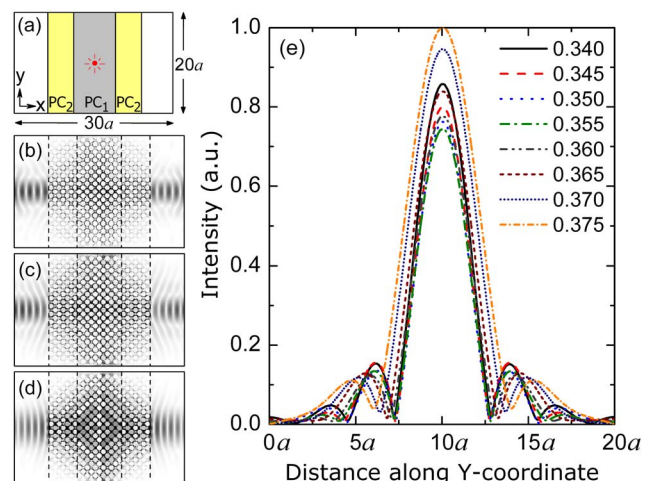


FIG. 4. (Color online) (a) Schematic of the PC composite used in the FDTD simulation. Simulated wave propagation inside the PC composite at a normalized frequency of (b) 0.340, (c) 0.355, and (d) 0.370. The light region and the dark one represent weak and strong amplitudes of the displacement field, respectively. (e) Simulated wave intensity at  $x=30a$  along the  $Y$  coordinate indicates that most acoustic waves at frequencies within  $\Delta f$  are confined at the center region after passing through the PC composite.

Quantitative analysis [Fig. 4(e)] based on the FDTD simulation results indicated that for all the frequencies in the collimation range ( $\Delta f$ ), most acoustic waves were confined at the center region after passing through the PC composite. Thus, the FDTD simulation results coincided with the PWE calculated results and confirmed that a PC composite can significantly enlarge the collimation region and cause wide-band acoustic collimation.

In conclusion, the collimation phenomena of PC composites were investigated numerically through both PWE and FDTD methods. The flatbands and the density of states near the collimation point were the key factors in determining the collimation characteristics of acoustic waves. An acoustic collimation lens composed of two PCs (steel cylinders in water) with different filling ratios was shown to enlarge the collimation region over a normalized frequency range by a factor of 185%–220%, thereby realizing wide-band acoustic collimation. The methodology described in this letter will prove useful in applications that require confined acoustic energy flow over long operation distances, such as acoustic imaging, drug delivery, cell sonoporation, and nondestructive evaluation.

We thank Dr. Tsung-Tsong Wu and Dr. Jia-Hong Sun for their help with the FDTD simulation, and gratefully acknowledge Dr. Bernhard R. Tittmann, Dr. Sabih I. Hayek, William Ames, Thomas R. Walker, and John R. Waldeisen for their help with the manuscript. This work was supported by the NSF NIRT grant (ECCS-0609128) and the start-up fund provided by The Pennsylvania State University.

- <sup>1</sup>K. M. Ho, C. T. Chan, and C. M. Soukoulis, *Phys. Rev. Lett.* **65**, 3152 (1990).
- <sup>2</sup>E. Yablonovitch and T. J. Gmitter, *Phys. Rev. Lett.* **67**, 2295 (1991).
- <sup>3</sup>P. V. Parimi, W. T. Lu, P. Vodo, J. Sokoloff, J. S. Derov, and S. Sridhar, *Phys. Rev. Lett.* **92**, 127401 (2004).
- <sup>4</sup>R. Moussa, S. Foteinopoulou, L. Zhang, G. Tuttle, K. Guven, E. Ozbay, and C. M. Soukoulis, *Phys. Rev. B* **71**, 085106 (2005).
- <sup>5</sup>I. Bulu, H. Caglayan, and E. Ozbay, *Phys. Rev. B* **72**, 045124 (2005).
- <sup>6</sup>S. L. He, Z. C. Ruan, L. Chen, and J. Q. Shen, *Phys. Rev. B* **70**, 115113 (2004).
- <sup>7</sup>M. Mojahedi, E. Schamiloglu, F. Hegeler, and K. J. Malloy, *Phys. Rev. E* **62**, 5758 (2000).
- <sup>8</sup>H. Kosaka, T. Kawashima, A. Tomita, M. Notomi, T. Tamamura, T. Sato, and S. Kawakami, *Appl. Phys. Lett.* **74**, 1212 (1999).
- <sup>9</sup>R. Iliiew, C. Etrich, and F. Lederer, *Opt. Express* **13**, 7076 (2005).
- <sup>10</sup>Z. L. Lu, C. A. Schuetz, S. Shi, C. Chen, G. P. Behrmann, and D. W. Prather, *IEEE Trans. Microwave Theory Tech.* **53**, 1362 (2005).
- <sup>11</sup>L. S. Chen, C. H. Kuo, and Z. Ye, *Appl. Phys. Lett.* **85**, 1072 (2004).
- <sup>12</sup>C. Qiu and Z. Liu, *Appl. Phys. Lett.* **89**, 063106 (2006).
- <sup>13</sup>M. S. Kushwaha, P. Halevi, L. Dobrzynski, and B. Djafari-Rouhani, *Phys. Rev. Lett.* **71**, 2022 (1993).
- <sup>14</sup>M. S. Kushwaha, P. Halevi, and G. Martinez, *Phys. Rev. B* **49**, 2313 (1994).
- <sup>15</sup>T. T. Wu, Z. G. Huang, and S. Lin, *Phys. Rev. B* **69**, 094301 (2004).
- <sup>16</sup>M. S. Kushwaha, *Appl. Phys. Lett.* **70**, 3218 (1997).
- <sup>17</sup>J. P. Berenger, *J. Comput. Phys.* **114**, 185 (1994).
- <sup>18</sup>J. H. Sun and T. T. Wu, *Phys. Rev. B* **71**, 174303 (2005).
- <sup>19</sup>K. Imamura and S. Tamura, *Phys. Rev. B* **70**, 174308 (2004).
- <sup>20</sup>S. Yang, J. H. Page, Z. Liu, M. L. Cowan, T. T. Chan, and P. Sheng, *Phys. Rev. Lett.* **93**, 024301 (2004).
- <sup>21</sup>X. Zhang and Z. Liu, *Appl. Phys. Lett.* **85**, 341 (2004).
- <sup>22</sup>N. Fang, D. Xi, J. Xu, M. Ambati, W. Srituravanich, C. Sun, and X. Zhang, *Nat. Mater.* **5**, 452 (2006).